2019

CarD and RbpA modify the kinetics of initial transcription and slow promoter escape of the Mycobacterium tuberculosis RNA polymerase

Drake Jensen

Ana R. Manzano

Christina L. Stallings

Eric A. Galburt

Published online 25 May 2019

Nucleic Acids Research, 2019, Vol. 47, No. 13 **6685–6698**
doi: 10.1093/nar/gkz449

CarD and RbpA modify the kinetics of initial transcription and slow promoter escape of the *Mycobacterium tuberculosis* RNA polymerase

Drake Jensen [1], Ana Ruiz Manzano[1], Jayan Rammohan[1], Christina L. Stallings[2] and Eric A. Galburt [1,*]

[1]Department of Biochemistry and Molecular Biophysics, Washington University School of Medicine, St. Louis, MO 63110, USA and [2]Department of Molecular Microbiology, Washington University School of Medicine, St. Louis, MO 63110, USA

Received February 01, 2019; Revised April 11, 2019; Editorial Decision May 08, 2019; Accepted May 09, 2019

ABSTRACT

The pathogen *Mycobacterium tuberculosis* (*Mtb*), the causative agent of tuberculosis, enacts unique transcriptional regulatory mechanisms when subjected to host-derived stresses. Initiation of transcription by the Mycobacterial RNA polymerase (RNAP) has previously been shown to exhibit different open complex kinetics and stabilities relative to *Escherichia coli* (*Eco*) RNAP. However, transcription initiation rates also depend on the kinetics following open complex formation such as initial nucleotide incorporation and subsequent promoter escape. Here, using a real-time fluorescence assay, we present the first in-depth kinetic analysis of initial transcription and promoter escape for the *Mtb* RNAP. We show that in relation to *Eco* RNAP, *Mtb* displays slower initial nucleotide incorporation but faster overall promoter escape kinetics on the *Mtb rrnA*P3 promoter. Furthermore, in the context of the essential transcription factors CarD and RbpA, *Mtb* promoter escape is slowed via differential effects on initially transcribing complexes. Finally, based on their ability to increase the rate of open complex formation and decrease the rate of promoter escape, we suggest that CarD and RbpA are capable of activation or repression depending on the rate-limiting step of a given promoter's basal initiation kinetics.

INTRODUCTION

Bacterial transcription initiation is a complex, multi-step process and is the major regulatory determinant for gene expression (1). Transcription is carried out by the RNA polymerase (RNAP) holoenzyme, consisting of the five subunit core RNAP ($\alpha_2\beta\beta'\omega$) and a σ subunit involved in specific promoter recognition (2). Extensive studies using *Escherichia coli* RNAP-σ^{70} holoenzyme (from here on referred to as *Eco* holo) have identified numerous kinetic intermediates involved in DNA-dependent RNA synthesis (outlined in Figure 1A). Transcription is initiated when RNAP holoenzyme (R) first binds duplex DNA promoter sequences (P) to form the closed complex (RP_c). Binding free energy then drives multiple conformational changes in both the RNAP and DNA that lead to the isomerization of RP_c to RP_o (open complex), where the duplex DNA is unwound around the transcription start site (TSS), resulting in an ∼13 base-pair (bp) single-stranded DNA bubble. After binding the initiating nucleotide, RNA polymerization begins as nucleotides (nt) complementary to the template DNA strand are incorporated into a growing RNA transcript resulting in an initial transcribing complex (RP_{itc}). In RP_{itc}, upstream contacts between RNAP and the promoter are static while downstream DNA is translocated into the enzyme, resulting in DNA scrunching (i.e. a growth of the DNA bubble) and possible abortive RNA synthesis where RNAP cycles through stages of short transcript production (3,4). Once 9–15 nt are incorporated into the RNA transcript, upstream contacts are broken, σ factor may dissociate, the transcription bubble shrinks, and RNAP fully escapes the promoter. This marks the end of initiation and the beginning of processive elongation (RP_e), where full-length transcripts are produced (5–7). From studies of *Eco* holo, numerous kinetic models have been put forth to describe promoter escape. In the most simplistic scheme, the pathway of promoter escape follows a sequential model where no off-pathway intermediates are generated prior to synthesis of full-length transcripts (Figure 1A – productive synthesis). Alternatively, branched models of promoter escape have been used to account for complexes that are unable to escape the promoter (i.e. moribund complexes) (8,9),

*To whom correspondence should be addressed. Tel: +1 314 362 5201; Fax: +1 314 362 7183; Email: egalburt@wustl.edu
Present address: Jayan Rammohan, National Institute of Standards and Technology (NIST), Gaithersburg, MD 20899, USA.

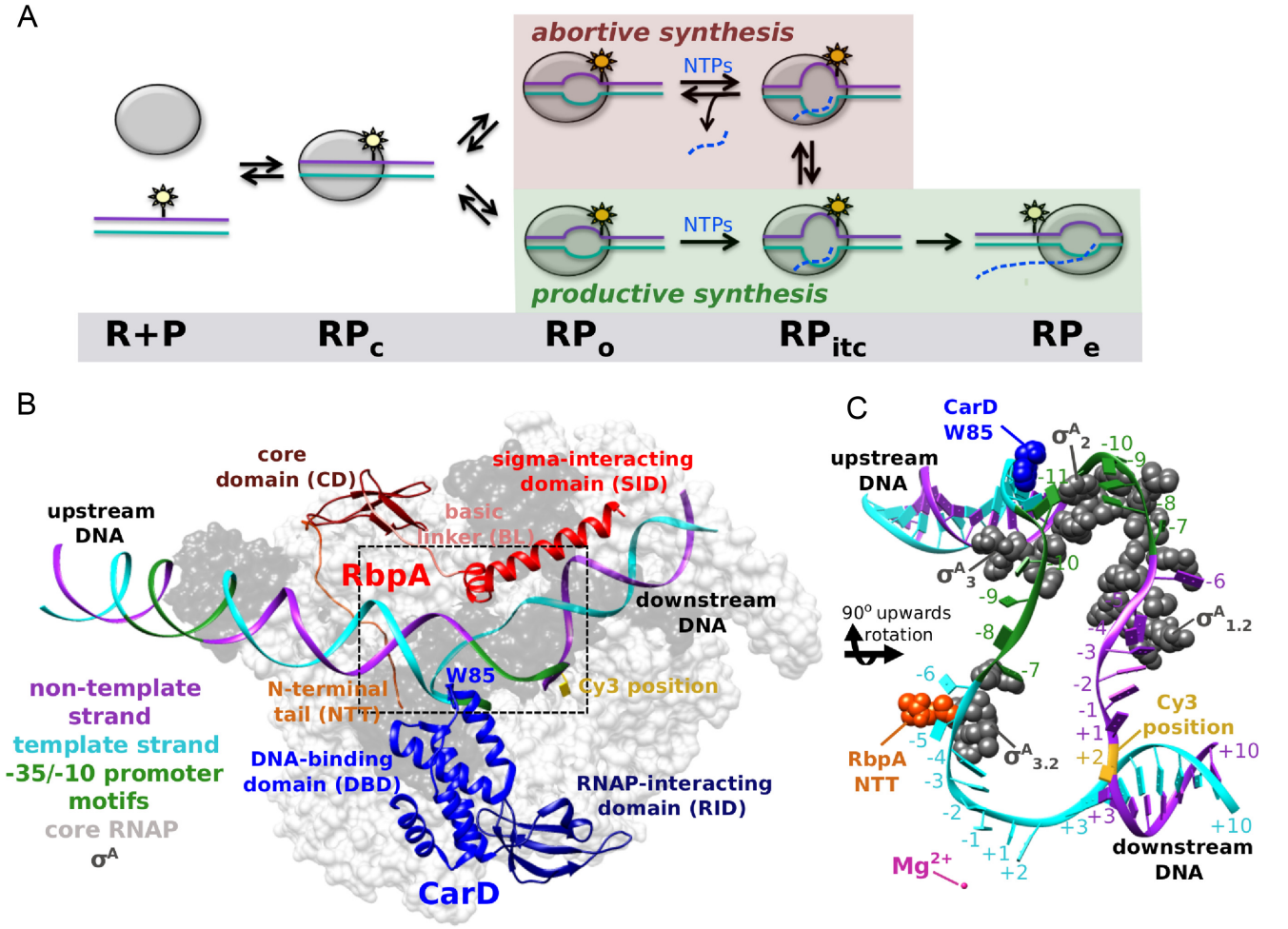

Figure 1. Schematic of bacterial transcription initiation and the structure of the *Mtb* RNAP-σ^A holoenzyme. (**A**) A kinetic model of initiation where the promoter DNA (P) containing the template strand (cyan) and non-template strand (purple) with a Cy3-fluorescent label positioned at the +2 position (yellow star) undergoes a fluorescence increase when RNAP (R, grey circle) unwinds the DNA during the isomerization from RP_c to RP_o. NTP addition results in scrunched RP_{itc} intermediates, where the open DNA bubble is increased in size. Transcription complexes can undergo either abortive cycling (red box) between RP_{itc} and RP_o states or productive synthesis (green box). Promoter escape leads to a fluorescence quenching when the DNA strands re-anneal in the vicinity of the Cy3-probe. (**B**) *Mtb* RNAP-σ^A holoenzyme *rrnA*P3 open promoter complex with CarD and RbpA (PDB: 6EDT) (30). Cryo-EM structure containing the *Mtb rrnA*P3 promoter (–60 to +30) with a fully open DNA bubble. Cy3-labeling position for use in stopped-flow experiments shown in yellow. Black box indicates a 90° rotation of the region shown in (**C**) where the predicted interactions of σ^A, CarD and RbpA with the open DNA bubble are shown. The Mg^{2+} ion indicates the position of the RNAP active site.

backtracked/paused complexes originating from RP_{itc} intermediates (10–12), as well as for cases where abortive initiation is not an on-pathway intermediate to an elongation complex and does not precede full-length transcription (13) (Figure 1A – abortive synthesis).

While much progress has been made to determine mechanistic details of *Eco* promoter escape, the kinetics and mechanism of mycobacterial promoter escape remains largely uncharacterized. To date, our kinetic studies on mycobacterial transcription have only focused on RP_o formation. Our results and those of others have indicated that the housekeeping *Mycobacterium bovis* RNAP-σ^A holoenzyme (*Mbo* holo), which differs in only one amino acid residue compared to *Mtb* RNAP-σ^A holoenzyme (*Mtb* holo), and *Eco* holo demonstrate dramatically different kinetics during the formation of RP_o on the *Mtb* ribosomal RNA (rRNA) *rrnA*P3 promoter (14,15). In contrast to *Eco*, which frequently forms a stable RP_o, *Mycobacterium, Bacillus* and *Thermus* RNAPs have been shown to form an unstable RP_o (14–18). Structural studies indicated that mycobacterial RNAPs and RNAPs from other Actinobacteria have unique insertions originating from the β' and σ^A subunits that may interfere with promoter DNA entry into the active site (19), providing a possible explanation for the lineage specific deficiency in RP_o stability. However, lineage specific structural insertions are common across bacterial core RNAP subunits and don't always lead to formation of an unstable RP_o; the insertions present in *E. coli* stabilize the open complex (20).

In addition to differences in the RNAP holoenzyme itself, Actinobacteria have unique transcription factors, including CarD and RbpA, which lead to a cooperative stabilization of the *rrnA*P3 RP_o (15,21), and as a result have been characterized as transcriptional activators. Neither CarD

or RbpA are present in *E. coli* (22), suggesting distinct strategies of transcriptional regulation across these bacterial species. *carD* and *rbpA* are up-regulated when subjected to bacterial stresses and are essential during growth under nutrient-rich conditions (22–26), suggesting roles in both maintaining cellular homeostasis and modulating *Mtb* gene expression to drive the pathogenesis of tuberculosis, the current leading cause of death from a single infectious agent. As RNAP is a direct target for first line antibiotics used to treat *Mtb* infection (27), further mechanistic studies of the unique mycobacterial transcription system is warranted and may lead to novel therapeutic strategies.

How CarD and RbpA interact with different components of the initiation complex has been elegantly elucidated via structural studies. Specifically, structures with σ^A-containing RNAP holoenzymes reveal that CarD and RbpA interact with both promoter DNA and RNAP (15,19,28–30). CarD consists of an N-terminal RNAP-interacting domain (RID) that binds the β-subunit of RNAP, a C-terminal DNA-binding domain (DBD) that makes non-specific contacts with promoter DNA, and a critical tryptophan residue (W85) that interacts with the upstream edge of the transcription bubble (22,28,30–32) (Figure 1B-C). Mutations in the RID that weaken the association with RNAP, the DBD or W85 can lead to increased sensitivity to antibiotics and decreased RP_o stability suggesting that all domains contribute to both biophysical and biological activities of CarD (14,16,31,33,34). RbpA consists of an N-terminal tail (NTT) that contacts RNAP β' and σ subunits, a core domain (CD) that contacts RNAP β', and a C-terminal sigma-interacting domain (SID). Separating the CD and SID is a basic linker (BL) region that interacts with promoter DNA just upstream of the −10 element (15,19,29,30,35) (Figure 1B and C). While both the BL and SID are necessary to promote a stable RP_o *in vitro,* removal of the NTT and the CD leads to enhanced RP_o stability relative to wild-type RbpA (25). However, *in vivo* RNA-sequencing analyses have indicated that the NTT and CD are responsible for a wide-ranging activation of gene expression, whereas the BL and SID can either activate or repress transcription depending on the promoter (25).

These RNA-sequencing results suggest that the current model of RbpA being solely defined as a transcriptional activator is not entirely correct. Working under the assumption that RbpA makes the same contacts with the RNAP holoenzyme regardless of which promoter is bound in the initiation complex, we hypothesized that for RbpA to also repress transcription, it must affect multiple kinetic intermediates during transcription initiation (36). For instance, by altering the stability of RP_o as well as the rate of promoter escape, transcription factors can exert differential regulatory outcomes (activation or repression) depending upon the rate-limiting kinetic transition for a given promoter (37,38). As RP_o stability has been shown to be inversely correlated with escape rates (39), direct measurements of the effects of transcription factors on escape are infrequently obtained despite the fact that the quantitative effect on escape can affect the regulatory outcome of the factor and represents an equally important step in gene regulation. As RbpA increases RP_o stability on the *rrnA*P3 promoter (15,21,25), we hypothesized that the transcriptional repression observed *in vivo* could be the result of RbpA delaying promoter escape. Similarly, as CarD also increases RP_o stability on *rrnA*P3 (14,15), we predicted that it also may slow promoter escape kinetics.

With the goals of understanding both the differences between *Eco* and *Mtb* transcriptional mechanisms and the effect that CarD and RpbA have on the overall rate of transcription initiation, we set out to determine both the basal and regulated rates of promoter escape for *Mtb*. Here, using a fluorescently labelled promoter construct that is sensitive to changes in DNA conformation (Figure 1A) (39), we measured the kinetics of promoter escape in a real-time stopped-flow assay. These transient kinetic measurements also allowed for detection of RP_{itc} intermediates; states that were previously unable to be observed given the dead-time of manual mixing techniques that have been employed to study *Eco* promoter escape (39). We show that in relation to *Eco*, *Mtb* displays faster escape kinetics on the *rrnA*P3 promoter, which can be delayed by both RbpA and CarD. By modelling changes in the rate of transcript production based on the factor-dependent effects on the kinetics of RP_o formation and promoter escape, we highlight the potential for RbpA and CarD to either up- or down-regulate transcript production depending on the basal rates of a given promoter. This new regulatory model for these factors highlights the possibility that CarD and RbpA can enact both transcriptional activation and repression to benefit *Mtb* persistence and survival.

MATERIALS AND METHODS

Preparation of fluorescent promoter DNA template

A 150 bp promoter template was generated containing the *rrnA*P3 promoter labelled with Cy3-NHS (Lumiprobe Corporation) attached to a C6-amine modified thymine on the +2 position of the non-template strand (for sequence, see *SI – Extended Methods*). For promoter preparation and labelling protocols, see (14).

Protein purification

Plasmids containing the *Mtb* H37Rv genomic DNA encoding for the different *Mtb* RNAP holoenzyme subunits were a generous gift from Dr. Mukhodpadhyay (Bose Institute, India) (40). Co-expression and purification of *Mtb* RNAP-σ^A holoenzyme was carried out in accordance with Prusa *et al.*, 2018. *Mtb* RbpA and CarD were expressed and purified as previously described (14,25). *Eco* RNAP-σ^{70} holoenzyme (catalogue #M0551S) was purchased from New England BioLabs, Inc.

Preparation of competitors to promote single-turnover conditions

Heparin sodium salt from porcine intestinal mucosa (MilliporeSigma) was dialyzed in transcription buffer (20 mM Tris (pH 8.0), 40 mM NaCl, 75 mM K-glutamate, 10 mM $MgCl_2$, 5 μM $ZnCl_2$, 20 μM EDTA). Heparin concentration was determined by standard curve titration with Azure A (41) and was repeated for each new lot of heparin purchased. Salmon-sperm DNA sheared to a maximum size of

2000 bp (Thermo Fisher Scientific) was buffer exchanged in transcription buffer and concentration was determined by A_{260}.

Stopped-flow fluorescence assays

All experiments were performed at 37°C using a SX-20 stopped-flow spectrophotometer (Applied Photophysics) with a dead time of ∼1 ms and total shot volume of ∼100 μl. Excitation was provided by a 535 nm fixed-wavelength LED light source with a 550 nm short pass cut-off filter (Applied Photophysics) and emission was monitored using a 570 nm long pass cut-off filter (Newport Optics). Accounting for all possible contributions from protein/DNA storage buffers, following equal volume mixing, the final reaction buffer conditions were as follows: 20 mM Tris (pH 8.0), 40 mM NaCl, 75 mM K-glutamate, 10 mM $MgCl_2$, 5 μM $ZnCl_2$, 20 μM EDTA, 5% (v/v) glycerol, 1 mM DTT, and 0.1 mg/ml BSA. For all experiments presented, at least two independent preparations of *Mtb* holo were used. Within each holoenzyme preparation, multiple technical replicates were combined to measure a 'shot average'. The shot averages from each holoenzyme preparation were weighted equally in determining the resultant averages and errors. Where applicable, error bars represent the standard error of the mean and statistical significance (P-value < 0.05) was determined using a two-sample t-Test with a 95% confidence interval (Origin Software).

Open complex formation. Prior to data acquisition, *Eco* holo or *Mtb* holo ± factors were incubated at 37°C for 10 min. Experiments were conducted by equal volume mixing of 2 nM *rrnA*P3 promoter Cy3-labelled DNA with 100 nM *Eco* holo or *Mtb* holo ± 4 μM RbpA, 2 μM CarD, or 4 μM RbpA and 2 μM CarD. Thus, final concentrations upon equal mixing were 1 nM DNA, 50 nM RNAP, 2 μM RbpA and 1 μM CarD. Data was collected for 250 s with logarithmic sampling over 2500 points. Each protein condition is represented by the average of at least five shots and plotted as fold-change over DNA alone according to the formula: $(F - F_o)/F_o$, where F_o is the buffer subtracted value for DNA alone and F is the buffer subtracted signal for DNA mixed with protein. $t_{1/2}{}^{open}$ values were calculated as the time at which it takes to reach half the maximal fluorescence amplitude. For RP_o formation experiments conducted in the presence of competitor, reaction conditions are identical as above except that 50 μg/mL salmon-sperm DNA was pre-incubated with 2 nM *rrnA*P3 promoter Cy3-labelled DNA.

Dissociation from open complex. 100 nM *Eco* holo or *Mtb* holo ± 4 μM RbpA, 2 μM CarD, or 4 μM RbpA and 2 μM CarD was incubated with 2 nM *rrnA*P3 promoter Cy3-labelled DNA at 37°C for 10 min. Dissociation of RNAP-promoter bound complexes was measured by subsequent equal volume mixing with various heparin or salmon-sperm DNA concentrations. Real-time traces were collected for 1000 sec on a logarithmic timescale, sampling either 2500 or 5000 points and were normalized to obtain the percentage of the initial signal remaining as a function of time with the formula: $[(F - F_o)/(F_{start} - F_o)] \times 100$, where F_o is the buffer subtracted value for DNA alone, F is the buffer subtracted signal, and F_{start} is the buffer subtracted signal at the beginning of the trace. This normalization did not affect the fitted fractional amplitudes or kinetics relative to the un-normalized buffer subtracted data itself (i.e. F, data not shown). Dissociation curves were fit to a sum of exponentials (two and three exponentials for salmon-sperm DNA and heparin experiments, respectively) using ProData Viewer (Applied Photophysics).

Promoter escape of open complexes under 'single-round' conditions. *Eco* holo or *Mtb* holo ± factors were pre-incubated with *rrnA*P3 DNA as in dissociation experiments and underwent equal volume mixing with various NTP (Thermo Fisher Scientific, catalogue #R0481) concentrations (50–2000 μM after mixing) and 50 μg/ml salmon-sperm DNA. Each condition is represented by at least a 5 shot average where data was acquired and normalized as in dissociation experiments. The fraction of inactive complexes, defined as those that didn't escape/dissociate from the DNA, was determined by the final fluorescence value following data normalization ($F_{inactive}$). At NTP concentrations of 50–100 μM, *Mtb* holo ± factors and *Eco* holo were fit to a sum of two and four exponential functions, respectively. At NTP concentrations higher than 100 μM, all traces required a sum of four exponentials for a reasonable fit. $t_{1/2}{}^{escape}$ values, as determined by the time needed to reach 50% of the signal difference between F_{start} and $F_{inactive}$ were calculated for conditions higher than 100 μM NTPs, where dissociation of *Mtb* holo RP_o was minimal relative to escape. The time required to reach the peak fluorescence amplitude following initial mixing (time-to-peak) was calculated by fitting each NTP-dependent promoter escape trace to a fifth order polynomial function from 0.0025 to 3 s (Origin Software). From the fits, the maximal peak amplitude was identified, and its corresponding time was obtained.

NTP subset experiments. NTP subset experiments were performed as in single-turnover promoter escape experiments except that select individual NTPs were added at a 1 mM final concentration to generate the RP_{itc} combinations outlined in Figure 4B. A chain terminating NTP analogue (3'-*O*-methyl-CTP, TriLink Biotechnologies, catalogue #N-1057) was used to generate at max a 5-mer RNA transcript. Conditions with 3'-O-methyl-CTP added are represented by a three shot average, whereas all other conditions are represented by at least a five shot average. Data was acquired for 3600 s to better obtain an estimate of the end point value for the percentage of signal remaining.

Time-to-peak kinetic simulations

Simulations were performed using KinTeK Global explorer (42). A three state, irreversible model ($RP_o \rightarrow RP_{itc} \rightarrow RP_e$) was used to model the promoter escape process to assess the time-to-peak and amplitude changes corresponding to an individual net entry (k_{itc}) or exit rate (k_{escape}) from initial transcribing intermediates. RP_{itc} was assigned a 10% higher observable fluorescence value in comparison to the starting RP_o signal, whereas RP_e lacked an observable fluorescence.

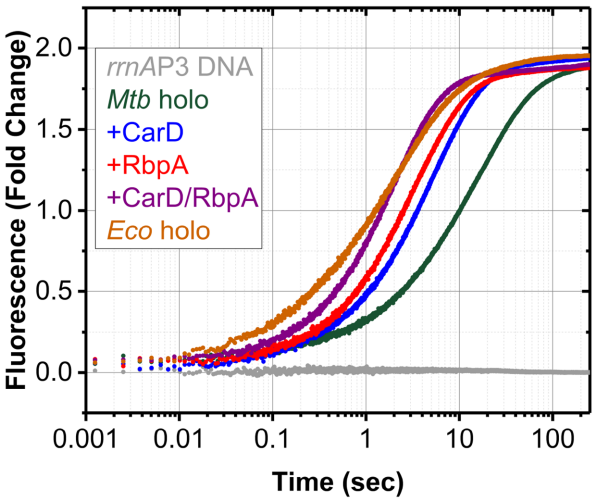

Figure 2. Real-time traces of RP_o formation as indicated by the increase in fluorescence relative to *rrnA*P3 DNA alone. Final concentrations are 50 nM *Eco* holo or *Mtb* holo with 1 μM CarD, 2 μM RbpA, or 1 μM CarD and 2 μM RbpA mixed with 1 nM *rrnA*P3 DNA. An average of five independent shots per condition is plotted as fold-change over DNA alone.

RESULTS

CarD and RbpA increase the rate of *Mtb* RNAP open complex formation

Use of a fluorescently labelled DNA construct containing the *Mtb rrnA*P3 promoter (see *SI – Extended Methods*) permitted us to monitor the events of transcription initiation in real-time (outlined in Figure 1A). Mixing *Mtb* and *Eco* holo with *rrnA*P3 promoter DNA (Materials and Methods) resulted in a rapid increase in the fluorescent signal as the duplex DNA was unwound around the position of the Cy3 fluorophore, indicative of RP_o formation (Figure 2). Addition of RNAP was required to observe this fluorescent signal, as only mixing CarD and RbpA against *rrnA*P3 promoter DNA resulted in no change relative to the DNA alone baseline (Supplementary Figure S1). Under these reaction conditions, which were optimized to saturate the final equilibrium fluorescence fold-change value (see *SI – Extended Methods*), we were unable to observe factor-dependent effects on RP_o stability. However, we were still able to extract kinetic information by calculating the time required to reach half the final fluorescence amplitude ($t_{1/2}^{open}$). When saturating amounts of CarD (1 μM, $t_{1/2}^{open} = 3.2 \pm 0.3$ s) and RbpA (2 μM, $t_{1/2}^{open} = 2.1 \pm 0.2$ s) were pre-incubated with *Mtb* holo and mixed with DNA, an increase in the rate of RP_o equilibration relative to *Mtb* holo alone ($t_{1/2}^{open} = 8.1 \pm 1.4$ s) was observed. Additionally, by pre-incubating both CarD and RbpA with *Mtb* holo ($t_{1/2}^{open} = 1.28 \pm 0.10$ s), similar kinetics to that of *Eco* holo without the addition of factor ($t_{1/2}^{open} = 1.12 \pm 0.04$ s) were obtained. These kinetic results are consistent with our previous observations obtained with *Mbo* holo under different reaction conditions (14,21). Furthermore, as the equilibrium fluorescence in these experiments was the same in the presence and absence of factors, direct effects from factor binding on the fluorescent signal can be excluded. This result is consistent with the structure of the factor-bound complexes that show the factors to be located on the other side of the DNA bubble compared to the Cy3-fluorophore (Figure 1C). Lastly, both CarD and RbpA display no kinetic effect on RP_o formation when pre-incubated with *Eco* holo, demonstrating RNAP specificity (Supplementary Figure S2). For *Mtb*CarD, this specificity is consistent with the known lineage-specific determinants of RID/RNAP interactions (43). For *Mtb*RbpA, this specificity has previously been reported using a hybrid RNAP holoenzyme containing *Eco* core subunits and *Mtb* σ^A (44). As both CarD and RbpA exhibit effects on the kinetics of *Mtb* RP_o formation, we hypothesized that they will also have an effect on *Mtb* promoter escape, given the additional RNAP and DNA contacts that will likely need to be broken for the RNAP to translocate away from the promoter.

Establishing single-turnover conditions: Heparin strips *Mtb* initiation complexes

To monitor promoter escape kinetics, we titrated NTPs to pre-formed *Mtb* RP_o, where the initial signal was now what was previously observed as the final equilibrium fluorescence in the RP_o formation experiments. In the absence of a competitor (i.e. RNAP trap), multiphasic kinetic behaviour was observed, where more than half of the initial signal remained 1000 s after NTP addition (Supplementary Figure S3). These results indicated potential rebinding to the promoter and subsequent RP_o formation by dissociated/escaped RNAPs and/or the presence of moribund complexes. To remove the possibility of promoter rebinding, we evaluated multiple competitors to promote single-turnover conditions. For *in vitro* studies of *E. coli* transcription, the polyanion heparin is commonly used to prevent (re)binding of free RNAP to promoter DNA (45). However, in titrating heparin against pre-formed *Mtb* RP_o (Materials and Methods), we were unable to find a heparin concentration at which the dissociation kinetics saturated (see *SI – Extended Methods,* Figure 3A, Supplementary Figures S4-S5), suggesting that heparin may be actively removing bound complexes (46). Alternatively, the use of a non-specific DNA competitor (salmon-sperm DNA), led to saturable dissociation kinetics (see *SI – Extended Methods,* Figure 3B, Supplementary Figure S5) and prevented initial binding to DNA quantitatively (see Materials and Methods, Supplementary Figure S6). This data supports that salmon-sperm DNA can be used to ensure single-turnover conditions for the study of NTP-dependent promoter escape of *Mtb* holo without actively promoting dissociation. For the reasons delineated above, we emphasize that for RNAP-promoter systems where there is an appreciable population of bound, but not open, complexes at equilibrium, heparin should be avoided as a competitor.

Identification of a transient peak signal at high NTP concentrations

As both escape ($RP_o \rightarrow RP_{itc} \rightarrow RP_e$) and dissociation ($RP_o \rightarrow RP_c \rightarrow R+P$) will result in a reduction of the fluorescence signal, it becomes essential that these two processes occur on different timescales to allow an accurate assessment of escape kinetics. Mixing *Mtb* holo *rrnA*P3 promoter

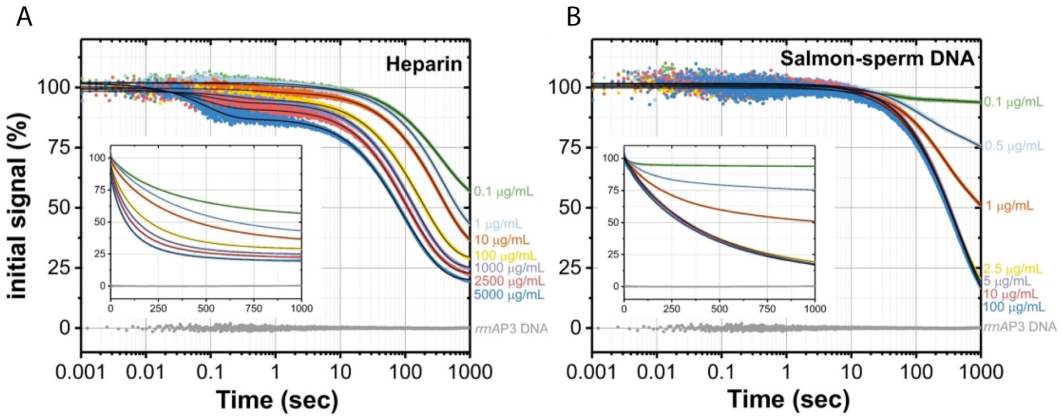

Figure 3. Dissociation from *Mtb* RP_o as a function of heparin and salmon-sperm DNA concentration. 50 nM *Mtb* holo pre-incubated with 1 nM *rrnA*P3 DNA titrated against various competitor concentrations (concentrations listed are following equal volume mixing). Data is plotted as percent of signal remaining at a given time. Averages of at least three shots are depicted. Black lines indicate fits to a sum of three exponentials for (**A**) heparin and a sum of two exponentials for (**B**) salmon-sperm DNA. Insets depict competitor titrations on a linear time-scale.

complexes with a low concentration of NTPs (50 μM) under single-turnover conditions yielded quenching of the fluorescent signal over time. However, this trace displayed very similar kinetics to the dissociation alone, no NTP, condition (Figure 4A). When we fit both the 0 and 50 μM NTP traces to a sum of two exponentials (Supplementary Figure S7A), the decay signals were dominated by the slower observed rate, mainly reporting on dissociative events (Supplementary Figure S8). With 100 μM NTPs, the slow observed rate no longer dominated the observed fluorescence amplitude (Supplementary Figure S8), suggesting that under these NTP concentrations promoter escape was now responsible for an appreciable fraction of the signal. Increasing to 1 mM NTPs led to ∼50-fold faster quenching kinetics compared to those observed without NTPs (Figure 4A), indicating that these high NTP concentrations are required for deconvolution of dissociation from promoter escape kinetics for *Mtb* holo.

In the presence of 1 mM NTPs, we unexpectedly observed a transient increase in fluorescence within the first second followed by the expected decay (Figure 4A, inset). These traces required at least four exponentials to obtain a reasonable fit (Supplementary Figure S7B). This peak was also present in both low (50 μM) and high (1 mM) NTP experiments with *Eco* holo (Supplementary Figure S9). Previous studies of *Eco* promoter escape using the same fluorescence readout described here with manual mixing techniques did not report the presence of a transient signal at 100 μM NTPs and were able to fit the escape traces to a sum of two exponentials (39,47). This discrepancy can be explained by the reduced dead-time of our stopped-flow assay (∼1 ms) compared to manual mixing techniques (>2 s). In agreement with these previous studies, only a two exponential fit was required to fit the 50 μM NTP condition starting at 2.5 s, while a four exponential fit was required when starting the fit at 1 ms for both 50 μM and 1 mM concentrations (Supplementary Figure S9). As this increase in the fluorescence becomes more prominent at high NTP concentrations and also occurs on similar timescales previously shown to correspond to short (3–10 mer) RNA synthesis (48) we hypothesized that the transient peak was due to a build-up of initiation intermediates, specifically, a subset of initially transcribing complexes (RP_{itc}).

The transient peak reports on initially transcribing complexes with RNA-DNA hybrids as short as 4 nt

A transient peak observed in the presence of NTPs could be generated by a population of RP_{itc} intermediates or via a further stabilization of RP_o. Since initiating nucleotides can stabilize the open DNA bubble (49–51), we asked whether mixing 1 mM GTP (Materials and Methods) with preformed *Mtb* RP_o led to an increase in signal. Under these reaction conditions, no fluorescence peak was detected as might be expected given the final equilibrium value in the absence of the initiating nucleotide was already saturated (Figure 2), although GTP binding could be observed via a reduction in the rate of dissociation (Figure 4B). This result showed that the transient peak was not due to an increase of RP_o stability. In contrast, when a maximal transcript length of 4 nucleotides (RP_{itc4}) was permitted by including 1 mM G/UTP, an increase in the fluorescence signal was observed (Figure 4B). No increase in fluorescence was observed by adding either G/ATP or G/CTP, indicating that the peak observed with the addition of G/UTP is not due to nucleotide mis-incorporation (Supplementary Figure S10). Addition of G/UTP and 3'-*O*-methyl-CTP, a NTP-analogue that has been shown to be effective in terminating the growth of the RNA chain in studies of *Eco* transcription (52) permitted us to monitor a 5-mer RNA product (RP_{itc5}). Relative to RP_{itc4}, RP_{itc5} displayed a further increase in the magnitude of the peak signal (Figure 4B). When a 9-mer (RP_{itc9}) RNA product was permitted by including 1 mM G/U/CTP, the magnitude of the peak signal was between that observed in the RP_{itc4} and RP_{itc5} conditions, suggesting that the maximal fluorescence amplitude corresponds to a population of initial transcribing complexes containing RNA-DNA hybrids between 4 and 9 nt in length (Figure 4B). In RP_{itc4}, RP_{itc5} and RP_{itc9} conditions, the same peak entry kinetics as compared to those in the presence of all 4 NTPs (RP_e) were observed (Figure 4B

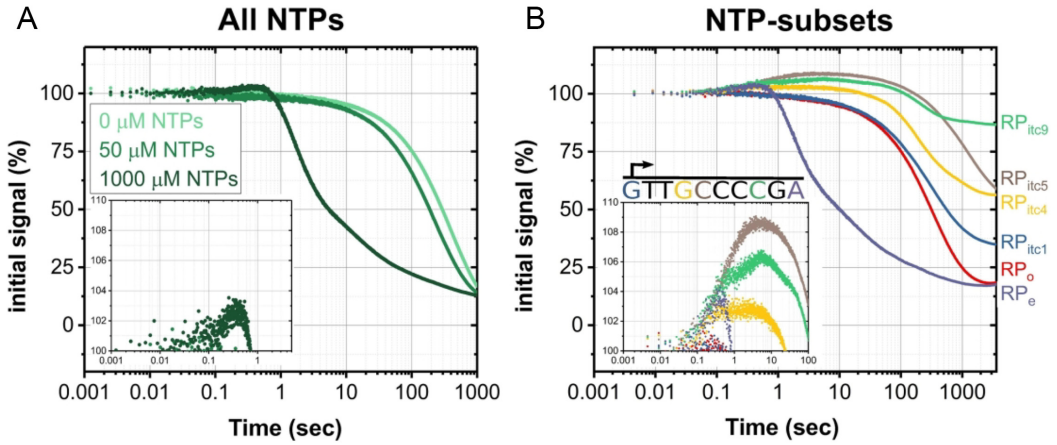

Figure 4. Transient peak signal present at high NTP concentrations is due to initial transcribing complexes. (**A**) Comparison of dissociation and promoter escape for *Mtb*. *Mtb* holo RP_o mixed with 25 μg/ml salmon-sperm DNA, 50 μM NTPs, and 1000 μM NTPs (concentrations following equal volume mixing). Inset shows the percent increase above the starting fluorescence signal plotted from 0.001 to 5 s. (**B**) NTP-subset experiments for *Mtb*. *Mtb* holo RP_o mixed with salmon-sperm DNA only (RP_o, red) or with salmon-sperm DNA and initiating nucleotide (GTP, RP_{itc1}, blue), nucleotides sufficient for formation of a 4-mer (G/UTP, RP_{itc4}, yellow), nucleotides sufficient for formation of a 5-mer (G/UTP and 3'-O-methyl-CTP, RP_{itc5}, brown), nucleotides sufficient for formation of a 9-mer (G/U/CTP, RP_{itc9}, green) or all four nucleotides to allow escape (RP_e, purple). NTP additions yielded a final concentration of 1000 μM for each NTP following equal volume mixing. Inset depicts peak signal plotted from 0.001 to 100 s with the initially transcribing sequence of the non-template strand listed above.

Inset). Performing identical NTP subset experiments with *Eco* holo displayed a similar trend to that of *Mtb* with respect to the RNA-DNA hybrid lengths required to observe a peak signal (Supplementary Figure S11), indicating that the increase in fluorescence reporting on RP_{itc} intermediates is not specific to *Mtb* RNAP. Combined, these results indicate a further enhancement of the fluorescence signal (distinct from that of RP_o) upon progression through the initial transcribing sequence for initially transcribing complexes with transcripts with as short 4 nt in length. Thus, the stopped-flow traces permit inferences regarding the rates of *both* initial nucleotide incorporation (through an evaluation of the peak signal) and promoter escape rates (through an evaluation of the fluorescence decay).

Mtb and *Eco* display different promoter escape kinetics

As rates of promoter escape are often anti-correlated with RP_o half-life, it is generally assumed that for a highly stable RP_o, the rate of promoter escape becomes limiting (53). As *Eco* forms a more stable RP_o on the *rrnA*P3 promoter than *Mtb* (14,15,21), we hypothesized that the rate of escape for *Eco* will be delayed relative to *Mtb*. Due to the complexity of the escape traces obtained at the 1 mM NTP condition (i.e. four observed rates (Supplementary Figures S7B, S9B) and inactive complexes that don't escape the promoter (Materials and Methods)), we chose to use $t_{1/2}^{escape}$ values (i.e. the time it takes for half of the *active* complexes to escape) to provide a semi-quantitative description of the escape kinetics. This type of analysis has been used previously to determine a single rate describing the overall promoter escape kinetics (k_E^{obs} defined as $1/t_{1/2}^{escape}$) (46,54,55). We emphasize that here k_E^{obs} is an average *observed rate* that reports on all the combined molecular processes involved in escape, including the rates of initial nucleotide incorporation, and should not be interpreted as an independent rate

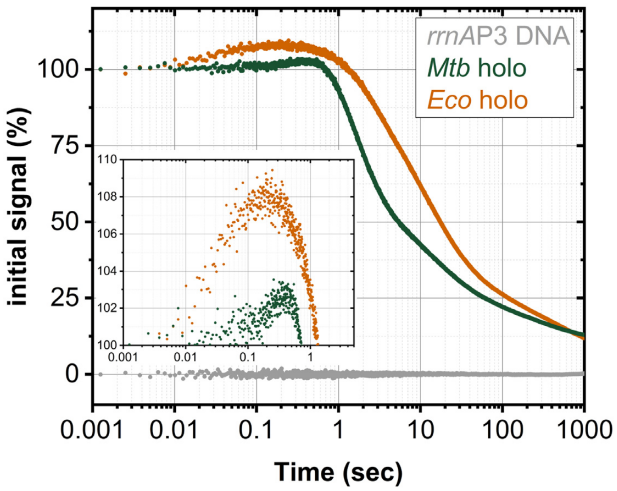

Figure 5. *Eco* displays faster initial nucleotide incorporation but slower promoter escape kinetics than *Mtb*. 50 nM *Mtb* (green) or *Eco* holo (orange) pre-incubated with 1 nM *rrnA*P3 DNA mixed with 25 μg/ml salmon-sperm DNA and 1 mM NTPs. Inset shows the percent increase above the starting fluorescence signal plotted between 0.001 and 5 s.

constant. As expected, *Eco* ($t_{1/2}^{escape} = 13.2 \pm 0.3$ s) exhibited roughly a 4-fold increase in the $t_{1/2}^{escape}$ value relative to *Mtb* ($t_{1/2}^{escape} = 3.7 \pm 0.2$ s), indicating slower overall escape kinetics (Figure 5). However, comparing the RP_{itc4}, RP_{itc5}, RP_{itc9}, and RP_e conditions, it is clear that entry into RP_{itc} intermediates always occurred on faster timescales for *Eco* holo (Figure 5, Supplementary Figure S12), indicating faster initial nucleotide incorporation kinetics. As *Eco* spends more time in the ensemble of RP_{itc} intermediate states than *Mtb* under NTP conditions that permit escape (Figure 5 Inset), these results indicate that the exit from

RP_{itc} intermediates for *Eco* is more rate-limiting compared to *Mtb*, leading to the slower k_E^{obs} relative to *Mtb*.

CarD and RbpA slow the rate of *Mtb* promoter escape

As both CarD and RbpA act to stabilize *Mtb* RP_o (14,15,21), we hypothesized that they should lead to a reduction in the rate of escape. To assess the effects of CarD and RbpA on the overall promoter escape kinetics, NTP titrations (Materials and Methods) were performed for *Mtb* holo in the absence and presence of saturating concentrations of each factor individually as well as with both factors combined (Figure 6A, Supplementary Figure S13). Increasing NTP concentrations led to a decrease in the $t_{1/2}^{escape}$ value (Supplementary Figure S14A) and a corresponding increase in the fractional amplitude of the faster decay rate (Supplementary Figure S8) in all cases. The $t_{1/2}$ escape analysis was limited to conditions of 250 μM NTPs or higher, where the remaining signal was nearly saturated (Supplementary Figure S14B) and the effects of NTP-independent dissociation of RNAP on the observed fluorescence signal were minimal. CarD, RbpA, and both factors combined all led to a decrease in the overall rate of escape. Specifically, in the presence of 1 mM NTPs the factors exhibited 2.9-, 1.4- and 2.4-fold increases in the $t_{1/2}^{escape}$ value respectively (Figure 6B and C). Additionally, large changes in the signal remaining were observed in the presence of CarD and RbpA (Figure 6B Inset, Supplementary Figure S14B). As this remaining signal is dependent upon both the NTP concentration and time of data acquisition (Supplementary Figure S14B-C), we only used conditions of saturating NTPs to ensure measurement of a signal representative of the reaction's true endpoint. This remaining signal was taken as a measurement of the fraction of initiation complexes that were unable to either dissociate or escape the promoter (i.e. the inactive fraction) as CarD and RbpA in the absence of RNAP do not alter the observed fluorescence signal (Supplementary Figure S1). These factor-dependent increases in inactive fraction correlate with factor-dependent increases in RP_o stability (21) where CarD, RbpA, and CarD/RbpA combined led to 2-, 1.8- and 2.8-fold increases in inactive fraction respectively compared to *Mtb* holo alone (Figure 6D).

The NTP-dependence of initial nucleotide incorporation as described by a three-state model

NTP titrations for *Mtb* holo and in the presence of factors yielded traces where the peak time and shape corresponding to RP_{itc} intermediates was dependent upon NTP concentration (Figure 6A Inset, Supplementary Figure S13 Insets). Specifically, the time required to reach the maximal peak amplitude (time-to-peak) decreased and the maximal peak amplitude increased as a function of NTP concentration (Figure 7A and B). To assess the NTP-dependence of the observed peak signal, we performed time-to-peak kinetic simulations using a three-state irreversible model ($RP_o \rightarrow RP_{itc} \rightarrow RP_e$) where the fluorescence increase is due to the population of molecules in the RP_{itc} state (Materials and Methods). These simulated traces can be used to test hypotheses regarding the NTP dependence of both the entry and exit rates from these intermediate states by comparing trends in the simulated traces to those observed experimentally. The first predictions of this model are that the net rate constant of RP_{itc} entry (i.e. $RP_o \rightarrow RP_{itc}$, k_{itc}) must be faster than the net rate constant of RP_{itc} exit (i.e. $RP_{itc} \rightarrow RP_e$, k_{escape}) to observe a peak signal (Supplementary Figure S15), and that increasing the net entry and exit rate constants by equal factors (i.e. both rates depend linearly on [NTP]) leads to a decrease in time-to-peak without a concomitant change in peak amplitude (Supplementary Figure S15B). In contrast, an NTP-dependent increase in the peak amplitude was observed for all conditions (Figure 7B), which could be simulated by either increasing k_{itc} or decreasing k_{escape} while removing the NTP dependence from the other net rate constant (Figure 7C and D, Supplementary Figures S16, S17). Of these models, only increasing k_{itc} led to the experimentally observed decrease in time-to-peak upon increasing [NTP] (Figure 7C, Supplementary Figure S16). Along these lines, we hypothesize that the rate-limiting step in *Mtb* promoter escape (k_{escape}) is an NTP-independent structural conversion from a late stage RP_{itc} intermediate to RP_e, such as σ^A repositioning or dissociation from the core RNAP (12).

CarD and RbpA have differential effects on RP_{itc} intermediates

To determine possible mechanisms by which CarD and RbpA slow promoter escape, we analysed factor-dependent changes in the peak signal corresponding to RP_{itc} intermediates. In the presence of all NTPs at the 1 mM condition (Figure 8A), CarD had the greatest effect on the peak signal with the slowest time-to-peak (Figure 7A) and the highest peak amplitude (Figure 7B). In the case of RbpA, a small, but significant (P-value = 0.042) increase in the time-to-peak relative to *Mtb* holo alone was observed (Figure 7A), with no statistically significant decrease in the peak amplitude (Figure 7B). In the presence of both factors, the time-to-peak increase was intermediate to that observed with CarD and RbpA separately (Figure 7A) and no significant change in the peak amplitude relative to *Mtb* holo alone was observed (Figure 7B). In summary, while the presence of factors always led to an increase in the time-to-peak, only CarD in the absence of RbpA led to an increase in the peak amplitude.

To explain these trends, we hypothesized that the factors affect the kinetics of RP_{itc} formation and escape differently. Using the three-state model of initial nucleotide incorporation, we asked whether we could replicate the experimentally observed peak signals in the presence of all NTPs and CarD and RbpA (Figure 8A). We found that reducing k_{escape} by the experimental fold-change in time-to-peak in the presence of CarD (0.4x) reproduced the CarD trend and that reducing k_{itc} by the experimental fold-change in time-to-peak in the presence of RbpA (0.9x) reproduced the RbpA data (Figure 8B). While the experimental trace in the presence of both factors is consistent with the slowing of both k_{itc} and k_{escape}, simply changing both net rates using the same fold changes as in the individual conditions for each factor did not replicate the peak signal (Figure 8B). However, decreasing both net rate constants equally

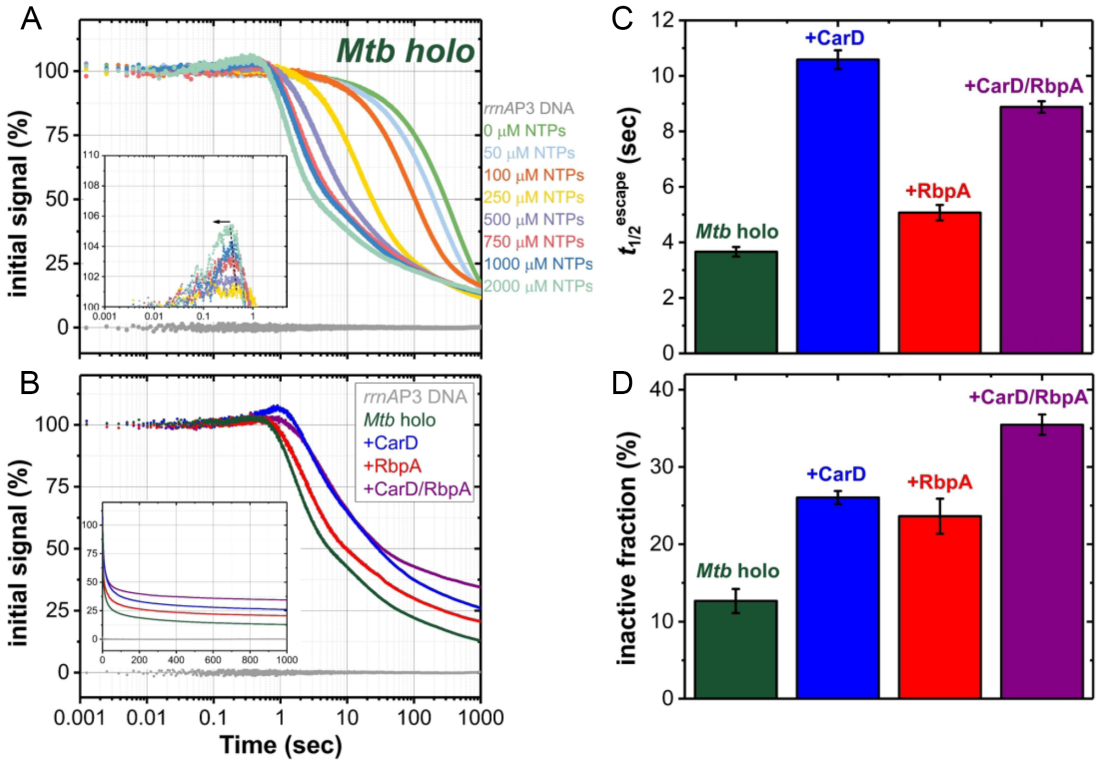

Figure 6. CarD and RbpA effects on *Mtb* promoter escape kinetics and inactive fraction. (**A**) NTP titrations for *Mtb* holo. NTP conditions range from 0 to 2 mM after equal volume mixing. Inset presents the transient peak signal as a percentage increase above the initial fluorescence value plotted from 0.001 to 5 s. Increasing the NTP concentration decreases the time-to-peak, as indicated by the dotted black line and arrow. (**B**) Overlay of escape traces conducted at 1 mM NTPs for *Mtb* holo ± factors. Inset depicts data on a linear time-scale. (**C**) Quantification of $t_{1/2}^{escape}$ values and (**D**) inactive fraction as calculated from the data in (B). Error bars represent standard errors of the mean.

(0.75x), yielded a time-to-peak and amplitude as observed experimentally (Figure 8B) suggesting that each factor is able to modulate either directly or indirectly the magnitude of the effect of the other factor. Based on this analysis, we conclude that CarD slows k_{escape} and RbpA slows k_{itc}.

DISCUSSION

Stopped-flow rapid mixing permits detection of RP_{itc} intermediates of bacterial transcription

The experiments described here were designed to measure the rates of promoter escape. Based on our previous use of this assay to study RP_o formation, we expected to observe only a fluorescence decay after the addition of NTPs as the polymerase moved downstream, permitting the Cy3-labelled region of the promoter to re-anneal around the transcription start site (TSS). In contrast, the traces exhibited a transient increase in fluorescence, which was detected on timescales not permitted with manual mixing techniques. Experiments with NTP-subsets revealed that the signal increase was due to initially transcribing intermediates with RNA–DNA hybrids as short as 4 nt, with a maximal fluorescence signal between 4 and 9 nt in length for both *Mtb* and *Eco* holo (Figure 4B, Supplementary Figure S11). Given the similarities in peak formation for these holoenzymes, we suggest that this technique can be broadly applicable in measuring initial nucleotide incorporation and escape kinetics for any bacterial RNAP. Additionally, as differences in the fluorescence signal were detected between RP_{itc4} and RP_{itc5} conditions (Figure 4B, Supplementary Figure S11), this technique permits detection of initial transcribing intermediates with nucleotide resolution at least within this range of RNA lengths. As escape from RP_{itc} intermediates is often rate limiting for transcription initiation (53), measurements of the kinetics and stabilities of these intermediates are of crucial importance in understanding gene expression mechanisms.

A three-state model to explain *Mtb* RP_{itc} intermediates

To explain the kinetics of RP_{itc} formation and escape for *Mtb* holo, a sequential, three-state model where k_{itc} (entry into RP_{itc} intermediates) is NTP-dependent and the rate-limiting k_{escape} (exit from RP_{itc} intermediates) is NTP-independent was able to replicate the observed trends in the peak signal as a function of NTP concentration (Figures 6A, 7A–C, Supplementary Figures S13, S16). An NTP-independent rate has been previously proposed from single-molecule studies evaluating the rate of exit from *Eco* RP_{itc6} paused-states on a consensus *lac* promoter, where it was suggested that pausing is not thermodynamically regulated by pre- and post-translocated states but rather is under kinetic control dictated by region 3.2 of *Eco* σ^{70} ($\sigma^{70}{}_{3.2}$) displacement from the active site (12).

While this sequential model proved useful to describe the entry and exit kinetics of *Mtb* RP_{itc} intermediates, we dis-

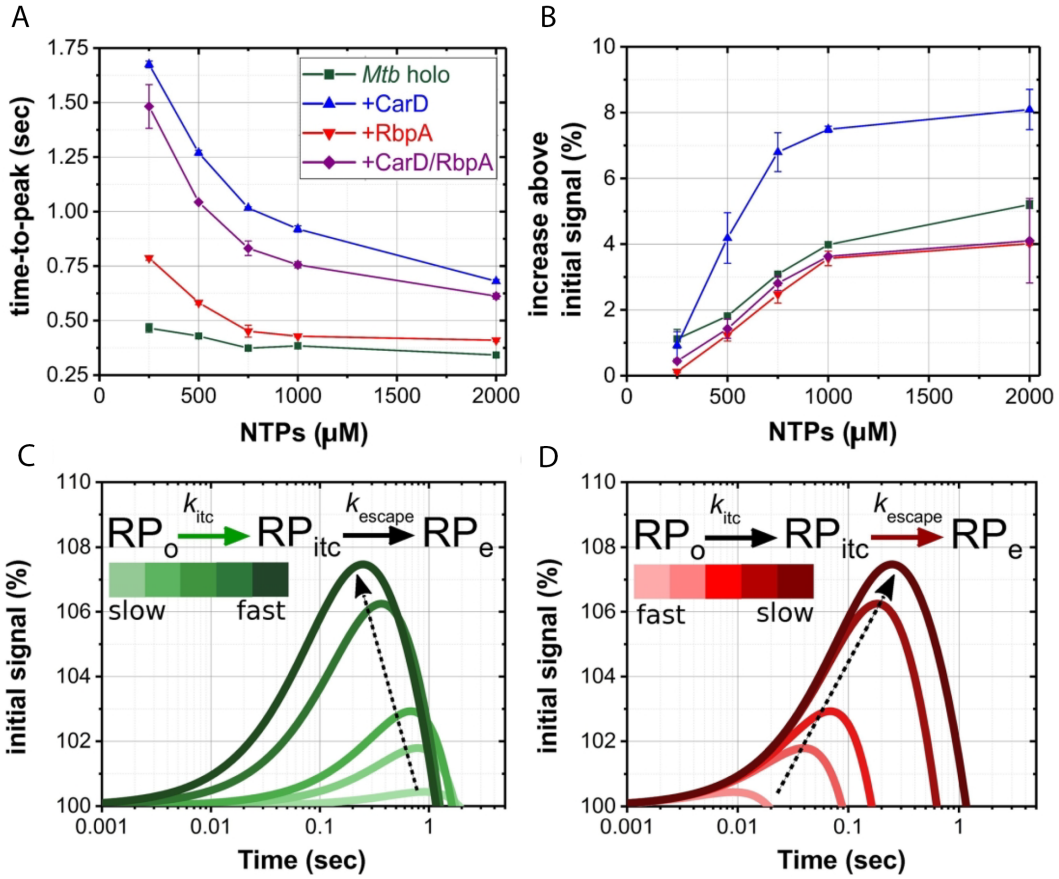

Figure 7. NTP dependence of the the peak signal. (**A**) Time-to-peak and (**B**) corresponding peak amplitudes as a function of NTP concentration for *Mtb* holo with and with-out factors. Error bars represent standard errors of the mean. (**C**) Time-to-peak simulations where the net exit rate is fixed while increasing the net entry rate into RP_{itc} and (**D**) the net entry rate is fixed while decreasing the net exit rate out-of RP_{itc} (see Supplementary Figures S16 and S17). Here, the darkening trend represents larger changes from the starting value and increases in the peak amplitude.

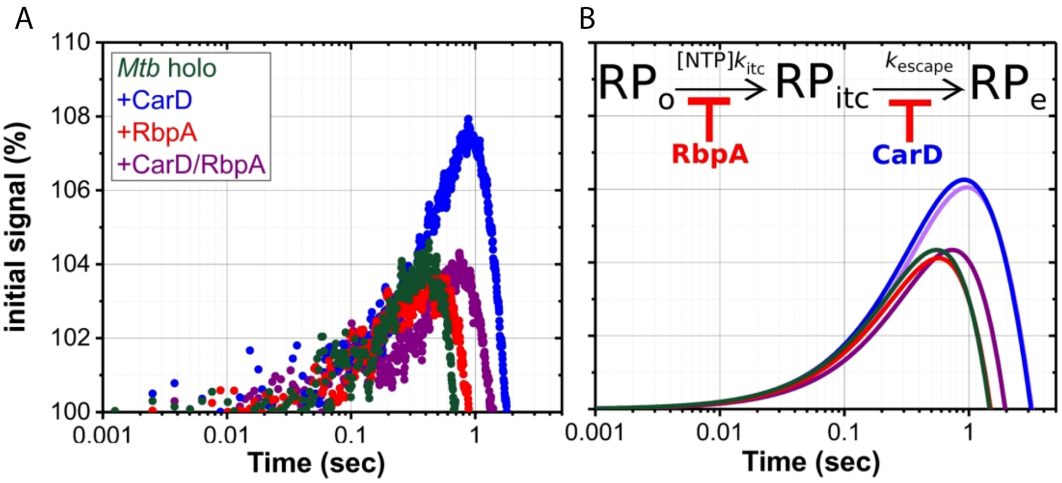

Figure 8. CarD and RbpA effects on RP_{itc} intermediates. (**A**) Overlay of peak signal obtained at 1 mM NTPs for *Mtb* holo ± factors plotted as a percentage increase above the initial fluorescence value. (**B**) Simulations of factor dependent effects on peak signal. The combined RP_o and RP_{itc} signals are plotted as a percent increase above the initial fluorescence signal. Factor dependent effects on k_{itc} and k_{escape} were adjusted according to the experimentally determined fold changes in the time-to-peak relative to *Mtb* holo alone. CarD (blue) is modeled by a 0.4-fold decrease in the net exit rate, RbpA (red) is modeled by a 0.9-fold decrease in the net entry rate. In the case of both factors, simulations adjusting both the net entry and exit rates as in the individual factor simulations were unable to reproduce the experimentally observed results in the time-to-peak and amplitude (light purple). Simulating a 0.75-fold decrease in both the net entry and exit rates, yielded a similar amplitude and time-to-peak as observed experimentally in the presence of both factors (dark purple).

courage the interpretation of the peak signal as a direct reporter of abortive RNA synthesis. As transitions within the ensemble of initial transcribing complexes have been proposed to occur both with and without release of abortive RNAs (12), we only interpret the peak signal as a reporter of RP_{itc} intermediates. Furthermore, we emphasize that this model is an oversimplification when evaluating the entire promoter escape process as it does not predict the phenomenon of promoter-bound inactive fractions. For *Mtb* holo, the signal remaining after dissociation in the absence of NTPs was nearly identical to that remaining after promoter escape in the presence of 1 mM NTPs (Figure 4, Supplementary Figure S14C), suggesting a mechanism where a subpopulation of unproductive or 'moribund' RP_o is not able to either dissociate or exhibit NTP-dependent escape on the time-scale of the experiment (9). This complicated kinetic behaviour is consistent with the existence of branched pathways that evolve on distinct time-scales (13). In addition, branched pathways due to inactivating processes like RNAP pausing and/or backtracking may exist during initial rounds of NTP incorporation (10–12), that could arise from the potential pause sequences within the initially transcribed sequence [(T/G) at +3/4 and (C/G) at +8/9] of the *rrnA*P3 promoter (47). As CarD and RbpA lead to a higher population of non-escaping complexes (Figure 6D), a potential regulatory mechanism resulting in repression, future work will focus on the sequence dependence of inactivation as well as the susceptibility of inactive complexes to cleavage factors. If inactivation of complexes arises from an increase in the backtracked fraction of initiation complexes, one expects this fraction of the inactive complexes to be reduced in the presence of *Mtb*Gre, an essential cleavage factor in mycobacteria (56), as is the case with GreB in studies of *Eco* transcription (10,55,57).

CarD and RbpA effects on RP_{itc} kinetics correlate with the location of their initiation complex contacts

CarD stabilizes RP_o by interacting with the upstream edge of the DNA bubble (Figure 1B-C) (28,30). These contacts do not need to be broken during initial nucleotide incorporation where RNAP presumably remains in a fixed position relative to upstream DNA (3,4). This is consistent with our model of CarD slowing k_{escape} while not affecting the NTP-dependent net rate constant, k_{itc}. RbpA also stabilizes RP_o by interacting with upstream promoter DNA, however, unlike CarD, RbpA also directly contacts σ (15,19,29,30,35). Specifically, the SID of RbpA contacts region 1.2, the non-conserved region (NCR), and region 2 of σ^A while the NTT of RbpA interacts with $\sigma^A{}_{3.2}$ (Figure 1B and C). In *E. coli*, $\sigma^{70}{}_{3.2}$ serves as an important regulatory determinant for abortive initiation as steric clashes within the RNA exit channel can lead to the release of abortive transcripts or to σ dissociation and escape (58–60). Furthermore, *Eco* $\sigma^{70}{}_{3.2}$ can stimulate phosphodiester bond formation via positioning of the template DNA strand (59). As the NTT of RbpA makes direct contacts with $\sigma^A{}_{3.2}$, we hypothesize that the NTT affects the mobility of the template DNA strand during initial rounds of nucleotide incorporation (29). This is consistent with previous work suggesting an RbpA effect on the selectivity of initiating substrates (61). Thus, the RbpA effects of slowing the NTP-dependent k_{itc} and overall escape kinetics on *rrnA*P3 measured here seem not to be driven by overcoming a higher energy barrier to escape provided by a RbpA-dependent increase in RP_o stability, but rather effects on spatial position of the promoter DNA within the active site.

The kinetic behaviour in the presence of both factors is not predicted from the cumulative effects of each factor alone. Qualitatively, the effect of RbpA on k_{itc} is potentiated in the presence of CarD and the effect of CarD on k_{escape} is mitigated in the presence of RbpA (Figure 8B). These results are consistent with the observed concomitant binding and cooperativity we observe in the kinetics of RP_o formation (21), and further suggests linkage between the factors, perhaps via the induction of different polymerase conformations. A complete mechanistic understanding will require future work with mutant factors to disentangle the domains responsible for factor-factor effects.

RbpA and CarD have the potential to both activate and repress transcription

Prior work has focused on quantifying transcription initiation kinetics on the *rrnA*P3 promoter up to RP_o formation. These experiments indicated that CarD serves to activate transcription by increasing the rate of DNA opening and slowing the rate of bubble collapse, thereby enhancing RP_o stability (14–16). RbpA, on the other hand, activates transcription by mainly increasing the rate of DNA opening, with little effect on the rate of closing (15,21,25). However, numerous transcription factors have been shown to affect both RP_o formation and promoter escape (37,62). For these factors, the regulatory outcome of factor binding (i.e. activation or repression) cannot be judged solely from effects on RP_o stability (53). In addition, RNA-sequencing data for RbpA (25) suggests that while functioning as an activator on a subset of promoters, RbpA is also able to repress transcription on a different promoter subset. This type of behavior has been well-established for the stringent response regulators *E. coli* DksA and ppGpp where the regulatory outcome depends upon the basal RP_o stability of a given promoter (63–65). CarD, RbpA, nor DksA are recruited to initiation complexes via sequence-dependent DNA contacts, suggesting indirect mechanisms for promoter-specific regulation.

We asked if a model based on our knowledge of the kinetics of RP_o formation and promoter escape (depicted in Figure 9A and discussed in *SI – Extended Methods*) would predict the ability of RbpA to either activate or repress transcription. This model assumes that RbpA increases the rate of RP_o formation and slows the rate of promoter escape on every promoter and that the resulting regulatory outcome depends on the limiting steps of a particular promoter's basal initiation kinetics. Using the calculated fold-changes in the rate of escape ($k_E{}^{obs}$ as determined by the $t_{1/2}{}^{escape}$ analysis) and RP_o equilibration in the presence of RbpA on the *rrnA*P3 promoter, we calculated the rate of transcription initiation for promoters with varying basal kinetics using an online resource we have developed (https://github.com/egalburt/transcript-flux-calculator) (36) (*SI – Extended Methods*). Consistent with our hypothesis, these

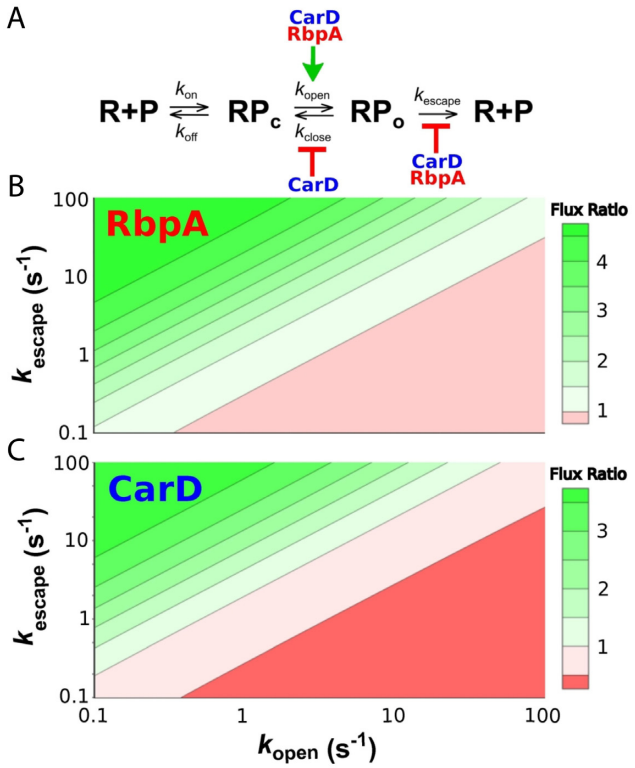

Figure 9. Differential regulation in flux is dependent upon the basal rates of initiation. (**A**) Three-state model for calculations of steady-state flux where CarD and RbpA either increase (green arrow) or decrease (red line) specific rate constants. Factor-dependent fold-changes in transcript flux show both activation (green) and repression (red) as a function of the basal opening and escape rates for (**B**) RbpA and (**C**) CarD. Promoters that are rate-limited at escape (i.e. fast k_{open}, slow k_{escape}) are predicted to be repressed, whereas promoters that are rate-limited at opening (i.e. slow k_{open}, fast k_{escape}) are predicted to be activated.

calculations reveal promoter-dependent differential regulation in transcript production rates (Figure 9B). Here, RbpA is predicted to repress transcription on promoters that are rate-limited at the escape step (i.e. form a stable RP_o) and activate transcription on promoters that are rate-limited by RP_o formation (i.e. *rrnA*P3). Even though RbpA only modestly slows escape kinetics, this effect on escape leads to predicted transcriptional repression across 3 orders of magnitude of k_{open} and k_{escape} basal rates. Furthermore, in comparing the calculated flux ratios to previously obtained RNA-sequencing data (25) showed that that modeled effects of RbpA determined by our *in vitro* kinetic analyses presented here can account for ∼70% of the predicted regulatory outcome determined *in vivo*, which could be increased to roughly 90% by modeling the kinetic effects of both RbpA and CarD combined (Supplementary Figure S18). As the presence of both factors on a single initiation complex may better represent physiological conditions and thus our RNA-sequencing data, the observed agreement between our kinetic modeling and the *in vivo* regulation suggests that that this simple model of regulation driven by a promoter's basal kinetics is sufficient to explain the majority of RbpA-dependent gene regulation. Thus, we propose that the promoter-dependent repression in the RNA-sequencing data is driven by the slowing of escape outweighing the activating effects of increasing the opening rate. Future kinetic studies on a variety of differentially regulated promoters identified in our RNA-sequencing analysis will directly test this hypothesis.

In the case of CarD, we have previously modeled a regulatory mechanism that assumed CarD slows the rate of escape and the rate of bubble collapse similarly (36). As we now have concrete evidence that CarD slows promoter escape, we used our experimentally derived fold-changes in the rate of escape and RP_o equilibration (*SI – Extended Methods*) and found that like RbpA, CarD also has the potential to both activate and repress transcription in a promoter specific manner (Figure 9C). Promoter specific motifs upstream of the TSS that confer stronger RNAP-promoter interactions, can lead to increased abortive cycling and inhibited full-length transcript synthesis (66,67). On such promoters where RP_o stability is high and escape is rate-limiting, our theoretical predictions suggest that CarD and RbpA would reduce the steady-state rate of transcript production. Additionally, CarD and RbpA both increase the inactive fraction of initiation complexes (Figure 6D), which would act to reduce transcript production directly, stochastically, and via a non-steady-state mechanism by blocking RNAP binding to a promoter for a long time relative to the rate of initiation. As a consequence, one might expect this mechanism to lead to fluctuations or bursts in the instantaneous rate of transcription initiation (68) and possibly account for the small fraction of genes predicted to be repressed *in vivo* by RbpA that fell outside the limits of our *in vitro* predictions that only accounted for kinetic regulation (Supplementary Figure S18).

DATA AVAILABILITY

Transcript flux calculations can be made using the online resources available at https://github.com/egalburt/transcript-flux-calculator.

SUPPLEMENTARY DATA

Supplementary Data are available at NAR Online.

ACKNOWLEDGEMENTS

The authors would like to thank Dr Eric J. Tomko for advice regarding experimental procedures and kinetic analyses, and Jerome Prusa and Dr Ashley L. Garner for contributions to the conceptual framework of this study.

FUNDING

National Institutes of Health [GM107544 to E.A.G. and C.L.S.]; Burroughs Wellcome Fund Investigator in the Pathogenesis of Infectious Disease Award [to C.L.S.]; Gary K. Ackers Fellowship and Elliot L. Elson Education and Training Fellowship [to D.J.]. Purchase of the stopped-flow fluorescence equipment was made possible by an equipment supplement from the National Institutes of Health [GM107544-04S1]. Funding for open access charge: National Institutes of Health [GM107544] and Washington University Departmental Support.

Conflict of interest statement. None declared.

REFERENCES

1. Browning,D.F. and Busby,S.J.W. (2016) Local and global regulation of transcription initiation in bacteria. *Nat. Rev. Microbiol.*, **14**, 638–650.
2. Feklístov,A., Sharon,B.D., Darst,S.A. and Gross,C.A. (2014) Bacterial sigma factors: a historical, structural, and genomic perspective. *Annu. Rev. Microbiol.*, **68**, 357–376.
3. Kapanidis,A.N., Margeat,E., Ho,S.O., Kortkhonjia,E., Weiss,S. and Ebright,R.H. (2006) Initial transcription by RNA polymerase proceeds through a DNA-scrunching mechanism. *Science*, **314**, 1144–1147.
4. Revyakin,A., Liu,C., Ebright,R.H. and Strick,T.R. (2006) Abortive initiation and productive initiation by RNA polymerase involve DNA scrunching. *Science*, **314**, 1139–1143.
5. Borukhov,S. and Nudler,E. (2008) RNA polymerase: the vehicle of transcription. *Trends Microbiol.*, **16**, 126–134.
6. Saecker,R.M., Record,M.T. and Dehaseth,P.L. (2011) Mechanism of bacterial transcription initiation: RNA polymerase - Promoter binding, isomerization to initiation-competent open complexes, and initiation of RNA synthesis. *J. Mol. Biol.*, **412**, 754–771.
7. Lee,J. and Borukhov,S. (2016) Bacterial RNA polymerase-DNA interaction—the driving force of gene expression and the target for drug action. *Front. Mol. Biosci.*, **3**, 73.
8. Susa,M., Sen,R. and Shimamoto,N. (2002) Generality of the branched pathway in transcription initiation by Escherichia coli RNA polymerase. *J. Biol. Chem.*, **277**, 15407–15412.
9. Vo,N. V., Hsu,L.M., Kane,C.M. and Chamberlin,M.J. (2003) In vitro studies of transcript initiation by Escherichia coli RNA polymerase. 2. Formation and characterization of two distinct classes of initial transcribing complexes. *Biochemistry*, **42**, 3787–3797.
10. Lerner,E., Chung,S., Allen,B.L., Wang,S., Lee,J., Lu,S.W., Grimaud,L.W., Ingargiola,A., Michalet,X., Alhadid,Y. *et al.* (2016) Backtracked and paused transcription initiation intermediate of Escherichia coli RNA polymerase. *Proc. Natl. Acad. Sci. U.S.A.*, **113**, E6562–E6571.
11. Duchi,D., Bauer,D.L. V, Fernandez,L., Evans,G., Robb,N., Hwang,L.C., Gryte,K., Tomescu,A., Zawadzki,P., Morichaud,Z. *et al.* (2016) RNA polymerase pausing during initial transcription. *Mol. Cell*, **63**, 939–950.
12. Dulin,D., Bauer,D.L. V, Bakermans,J.J.W., Kaller,M., Morichaud,Z., Petushkov,I., Depken,M., Brodolin,K. and Kapanidis,A.N. (2018) Pausing controls branching between productive and non-productive pathways during initial transcription. *Nat. Commun.*, **9**, 1478.
13. Henderson,K.L., Felth,L.C., Molzahn,C.M., Shkel,I., Wang,S., Chhabra,M., Ruff,E.F., Bieter,L., Kraft,J.E. and Record,M.T. (2017) Mechanism of transcription initiation and promoter escape by E. coli RNA polymerase. *Proc. Natl. Acad. Sci. U.S.A.*, **114**, E3032–E3040.
14. Rammohan,J., Ruiz Manzano,A., Garner,A.L., Stallings,C.L. and Galburt,E.A. (2015) CarD stabilizes mycobacterial open complexes via a two-tiered kinetic mechanism. *Nucleic Acids Res.*, **43**, 3272–3285.
15. Hubin,E.A., Fay,A., Xu,C., Bean,J.M., Saecker,R.M., Glickman,M.S., Darst,S.A. and Campbell,E.A. (2017) Structure and function of the mycobacterial transcription initiation complex with the essential regulator RbpA. *Elife*, **6**, e22520.
16. Davis,E., Chen,J., Leon,K., Darst,S.A. and Campbell,E.A. (2015) Mycobacterial RNA polymerase forms unstable open promoter complexes that are stabilized by CarD. *Nucleic Acids Res.*, **43**, 433–445.
17. Whipple,F.W. and Sonenshein,A.L. (1992) Mechanism of initiation of transcription by Bacillus subtilis RNA polymerase at several promoters. *J. Mol. Biol.*, **223**, 399–414.
18. Xue,Y., Hogan,B.P. and Erie,D.A. (2000) Purification and initial characterization of RNA polymerase from thermus thermophilus strain HB8. *Biochemistry*, **39**, 14356–14362.
19. Hubin,E.A., Lilic,M., Darst,S.A. and Campbell,E.A. (2017) Structural insights into the mycobacteria transcription initiation complex from analysis of X-ray crystal structures. *Nat. Commun.*, **8**, 16072.
20. Artsimovitch,I., Svetlov,V., Murakami,K.S. and Landick,R. (2003) Co-overexpression of Escherichia coli RNA polymerase subunits allows isolation and analysis of mutant enzymes lacking lineage-specific sequence insertions. *J. Biol. Chem.*, **278**, 12344–12355.
21. Rammohan,J., Ruiz Manzano,A., Garner,A.L., Prusa,J., Stallings,C.L. and Galburt,E.A. (2016) Cooperative stabilization of Mycobacterium tuberculosis rrnAP3 promoter open complexes by RbpA and CarD. *Nucleic Acids Res.*, **44**, 7304–7313.
22. Stallings,C.L., Stephanou,N.C., Chu,L., Hochschild,A., Nickels,B.E. and Glickman,M.S. (2009) CarD is an essential regulator of rRNA transcription required for mycobacterium tuberculosis persistence. *Cell*, **138**, 146–159.
23. Betts,J.C., Lukey,P.T., Robb,L.C., McAdam,R.A. and Duncan,K. (2002) Evaluation of a nutrient starvation model of Mycobacterium tuberculosis persistence by gene and protein expression profiling. *Mol. Microbiol.*, **43**, 717–731.
24. Bortoluzzi,A., Muskett,F.W., Waters,L.C., Addis,P.W., Rieck,B., Munder,T., Schleier,S., Forti,F., Ghisotti,D., Carr,M.D. *et al.* (2013) Mycobacterium tuberculosis RNA polymerase-binding protein A (RbpA) and its interactions with sigma factors. *J. Biol. Chem.*, **288**, 14438–14450.
25. Prusa,J., Jensen,D., Santiago-Collazo,G., Pope,S.S., Garner,A.L., Miller,J.J., Ruiz Manzano,A., Galburt,E.A. and Stallings,C.L. (2018) Domains within RbpA serve specific functional roles that regulate the expression of distinct mycobacterial gene subsets. *J. Bacteriol.*, **200**, e00690-17.
26. Forti,F., Mauri,V., Deh,G. and Ghisotti,D. (2011) Isolation of conditional expression mutants in Mycobacterium tuberculosis by transposon mutagenesis. *Tuberculosis*, **91**, 569–578.
27. Ma,C., Yang,X. and Lewis,P.J. (2016) Bacterial transcription as a target for antibacterial drug development. *Microbiol. Mol. Biol. Rev.*, **80**, 139–160.
28. Bae,B., Chen,J., Davis,E., Leon,K., Darst,S.A. and Campbell,E.A. (2015) CarD uses a minor groove wedge mechanism to stabilize the RNA polymerase open promoter complex. *Elife*, **4**, e08505.
29. Boyaci,H., Chen,J., Lilic,M., Palka,M., Mooney,R.A., Landick,R., Darst,S.A. and Campbell,E.A. (2018) Fidaxomicin jams Mycobacterium tuberculosis RNA polymerase motions needed for initiation via RbpA contacts. *Elife*, **7**, e34823.
30. Boyaci,H., Chen,J., Jansen,R., Darst,S.A. and Campbell,E.A. (2019) Structures of an RNA polymerase promoter melting intermediate elucidate DNA unwinding. *Nature*, **565**, 382–385.
31. Srivastava,D.B., Leon,K., Osmundson,J., Garner,A.L., Weiss,L.A., Westblade,L.F., Glickman,M.S., Landick,R., Darst,S.A., Stallings,C.L. *et al.* (2013) Structure and function of CarD, an essential mycobacterial transcription factor. *Proc. Natl. Acad. Sci. U.S.A.*, **110**, 12619–12624.
32. Gulten,G. and Sacchettini,J.C. (2013) Structure of the Mtb CarD/RNAP β-lobes complex reveals the molecular basis of interaction and presents a distinct DNA-binding domain for Mtb CarD. *Structure*, **21**, 1859–1869.
33. Weiss,L.A., Harrison,P.G., Nickels,B.E., Glickman,M.S., Campbell,E.A., Darst,S.A. and Stallings,C.L. (2012) Interaction of CarD with RNA polymerase mediates Mycobacterium tuberculosis viability, rifampin resistance, and pathogenesis. *J. Bacteriol.*, **194**, 5621–5631.
34. Garner,A.L., Weiss,L.A., Ruiz Manzano,A., Galburt,E.A. and Stallings,C.L. (2014) CarD integrates three functional modules to promote efficient transcription, antibiotic tolerance, and pathogenesis in mycobacteria. *Mol. Microbiol.*, **93**, 682–697.
35. Hubin,E.A., Tabib-Salazar,A., Humphrey,L.J., Flack,J.E., Olinares,P.D.B., Darst,S.A., Campbell,E.A. and Paget,M.S. (2015) Structural, functional, and genetic analyses of the actinobacterial transcription factor RbpA. *Proc. Natl. Acad. Sci. U.S.A.*, **112**, 7171–7176.
36. Galburt,E.A. (2018) The calculation of transcript flux ratios reveals single regulatory mechanisms capable of activation and repression. *Proc. Natl. Acad. Sci. U.S.A.*, **115**, E11604–E11613.
37. Monslave,M., Calles,B., Mencıa,M., Salas,M. and Rojo,F. (1997) Transcription activation or repression by Phage psi 29 protein p4 depends on the strength of the RNA polymerase – promoter interactions. *Mol. Cell*, **1**, 99–107.
38. Hochschild,A. and Dove,S.L. (1998) Protein-protein contacts that activate and repress prokaryotic transcription. *Cell*, **92**, 597–600.

39. Ko,J. and Heyduk,T. (2014) Kinetics of promoter escape by bacterial RNA polymerase: effects of promoter contacts and transcription bubble collapse. *Biochem. J.*, **463**, 135–144.
40. Banerjee,R., Rudra,P., Prajapati,R.K., Sengupta,S. and Mukhopadhyay,J. (2014) Optimization of recombinant Mycobacterium tuberculosis RNA polymerase expression and purification. *Tuberculosis*, **94**, 397–404.
41. Mascotti,D.P. and Lohman,T.M. (1995) Thermodynamics of charged Oligopeptide-Heparin interactions. *Biochemistry*, **34**, 2908–2915.
42. Johnson,K.A., Simpson,Z.B. and Blom,T. (2009) Global kinetic explorer: a new computer program for dynamic simulation and fitting of kinetic data. *Anal. Biochem.*, **387**, 20–29.
43. Westblade,L.F., Campbell,E.A., Pukhrambam,C., Padovan,J.C., Nickels,B.E., Lamour,V. and Darst,S.A. (2010) Structural basis for the bacterial transcription-repair coupling factor/RNA polymerase interaction. *Nucleic Acids Res.*, **38**, 8357–8369.
44. Hu,Y., Morichaud,Z., Chen,S., Leonetti,J.-P. and Brodolin,K. (2012) Mycobacterium tuberculosis RbpA protein is a new type of transcriptional activator that stabilizes the σ^A-containing RNA polymerase holoenzyme. *Nucleic Acids Res.*, **40**, 6547–6557.
45. Ross,W. and Gourse,R.L. (2009) Analysis of RNA polymerase-promoter complex formation. *Methods*, **47**, 13–24.
46. Pfeffer,S.R., Stahl,S.J. and Chamberlin,M.J. (1977) Binding of Escherichia coli RNA Polymerase to T7 DNA: displacement of Holoenzyme from Promoter Complexes by Heparin. *J. Biol. Chem.*, **252**, 5403–5407.
47. Heyduk,E. and Heyduk,T. (2018) DNA template sequence control of bacterial RNA polymerase escape from the promoter. *Nucleic Acids Res.*, **46**, 4469–4486.
48. Henderson,K., Evensen,C.E., Molzahn,C., Felth,L.C., Dyke,S., Liao,G., Shkel,I.A. and Record,M.T. (2019) RNA Polymerase: Step by step kinetics and mechanism of transcription initiation. *Biochemistry*, **58**, 2339–2352.
49. Tare,P., China,A. and Nagaraja,V. (2012) Distinct and contrasting transcription initiation patterns at mycobacterium tuberculosis promoters. *PLoS One*, **7**, e43900.
50. Gaal,T., Bartlett,M.S., Ross,W., Turnbough,C.L. and Gourse,R.L. (1997) Transcription regulation by initiating NTP concentration: rRNA synthesis in bacteria. *Science*, **278**, 2092–2097.
51. China,A., Tare,P. and Nagaraja,V. (2010) Comparison of promoter-specific events during transcription initiation in mycobacteria. *Microbiology*, **156**, 1942–1952.
52. Fu,T., Geiduschek,E.P. and Kassavetis,G.A. (1998) Abortive initiation of transcription at a hybrid promoter: an analysis of the sliding clamp activator of bacteriophage T4 late transcription, and a comparison of the σ70 and T4 GP55 promoter recognition proteins. *J. Biol. Chem.*, **273**, 34042–34048.
53. Hsu,L.M. (2002) Promoter clearance and escape in prokaryotes. *Biochim. Biophys. Acta*, **1577**, 191–207.
54. Strainic,M.G., Sullivan,J.J., Velevis,A. and DeHaseth,P.L. (1998) Promoter recognition by Escherichia coli RNA polymerase: Effects of the UP element on open complex formation and promoter clearance. *Biochemistry*, **37**, 18074–18080.
55. Petushkov,I., Esyunina,D., Mekler,V., Severinov,K., Pupov,D. and Kulbachinsky,A. (2017) Interplay between σ region 3.2 and secondary channel factors during promoter escape by bacterial RNA polymerase. *Biochem. J.*, **474**, 4053–4064.
56. China,A., Mishra,S. and Nagaraja,V. (2011) A transcript cleavage factor of mycobacterium tuberculosis important for its survival. *PLoS One*, **6**, e21941.
57. Lass-Napiorkowska,A. and Heyduk,T. (2016) Real-Time observation of backtracking by bacterial RNA polymerase. *Biochemistry*, **55**, 647–658.
58. Pupov,D., Kuzin,I., Bass,I. and Kulbachinskiy,A. (2014) Distinct functions of the RNA polymerase σ subunit region 3.2 in RNA priming and promoter escape. *Nucleic Acids Res.*, **42**, 4494–4504.
59. Kulbachinskiy,A. and Mustaev,A. (2006) Region 3.2 of the σ subunit contributes to the binding of the 3′-initiating nucleotide in the RNA polymerase active center and facilitates promoter clearance during initiation. *J. Biol. Chem.*, **281**, 18273–18276.
60. Cashel,M., Hsu,L.M. and Hernandez,V.J. (2003) Changes in conserved region 3 of Escherichia coli σ70 reduce abortive transcription and enhance promoter escape. *J. Biol. Chem.*, **278**, 5539–5547.
61. Sudalaiyadum Perumal,A., Vishwakarma,R.K., Hu,Y., Morichaud,Z. and Brodolin,K. (2018) RbpA relaxes promoter selectivity of M. tuberculosis RNA polymerase. *Nucleic Acids Res.*, **46**, 10106–10118.
62. Smith,T.L. and Sauer,R.T. (1996) Dual regulation of open-complex formation and promoter clearance by Arc explains a novel repressor to activator switch. *Proc. Natl. Acad. Sci. U.S.A.*, **93**, 8868–8872.
63. Paul,B.J., Berkmen,M.B. and Gourse,R.L. (2005) DksA potentiates direct activation of amino acid promoters by ppGpp. *Proc. Natl. Acad. Sci. U.S.A.*, **102**, 7823–7828.
64. Barker,M.M., Gaal,T., Josaitis,C.A. and Gourse,R.L. (2001) Mechanism of regulation of transcription initiation by ppGpp. I. Effects of ppGpp on transcription initiation in vivo and in vitro. *J. Mol. Biol.*, **305**, 673–688.
65. Sanchez-Vazquez,P., Dewey,C.N., Kitten,N., Ross,W. and Gourse,R.L. (2019) Genome-wide effects on *Escherichia coli* transcription from ppGpp binding to its two sites on RNA polymerase. Gottesman,S (ed). *Proceedings of the National Academy of Sciences of the United States of America*. Vol. **116**, pp. 8310–8319.
66. Ellinger,T., Behnke,D., Bujard,H. and Gralla,J.D. (1994) Stalling of Escherichia coli RNA polymerase in the +6 to +12 region in vivo is associated with tight binding to consensus promoter elements. *J. Mol. Biol.*, **239**, 455–465.
67. Vo,N. V., Hsu,L.M., Kane,C.M. and Chamberlin,M.J. (2003) In vitro studies of transcript initiation by Escherichia coli RNA polymerase. 3. Influences of individual DNA elements within the promoter recognition region on abortive initiation and promoter escape. *Biochemistry*, **42**, 3798–3811.
68. Mitarai,N., Dodd,I.B., Crooks,M.T. and Sneppen,K. (2008) The generation of promoter-mediated transcriptional noise in bacteria. *PLoS Comput. Biol.*, **4**, e1000109.